The Astrophysical Journal Letters, 976:L20 (10pp), 2024 December 1 https://doi.org/10.3847/2041-8213/ad85da

GRB 240529A: A Tale of Two Shocks

Tian-Rui Sun[1], Jin-Jun Geng[1], Jing-Zhi Yan[1], You-Dong Hu[2,3], Xue-Feng Wu[1,4], Alberto J. Castro-Tirado[3,5], Chao Yang[1], Yi-Ding Ping[1], Chen-Ran Hu[6], Fan Xu[6], Hao-Xuan Gao[1], Ji-An Jiang[4,7], Yan-Tian Zhu[1,4], Yongquan Xue[8,4], Ignacio Pérez-García[3], Si-Yu Wu[3], Emilio Fernández-García[3], María D. Caballero-García[3], Rubén Sánchez-Ramírez[3], Sergiy Guziy[3,9,10], I. Olivares[3], Carlos Jesus Pérez del Pulgar[5], A. Castellón[5,11], S. Castillo[12], Ding-Rong Xiong[13], Shashi B. Pandey[14], David Hiriart[15], Guillermo García-Segura[15,3], William H. Lee[16], I. M. Carrasco-García[17], Il H. Park[18], S. Jeong[19], Petrus J. Meintjes[20], Hendrik J. van Heerden[20], Antonio Martín-Carrillo[21], Lorraine Hanlon[21], Bin-Bin Zhang[6,22], L. Hernández-García[23,24,25], Maria Gritsevich[26,27,28], Andrea Rossi[29], Elisabetta Maiorano[29], Felice Cusano[29], Paolo D'Avanzo[2], Matteo Ferro[30,2], Andrea Melandri[31], Massimiliano De Pasquale[32], Riccardo Brivio[2,30], Min Fang[1], Lu-Lu Fan[8,4,33], Wei-Da Hu[34,35], Zhen Wan[8,4], Lei Hu[36], Ying-Xi Zuo[1], Jin-Long Tang[37], Xiao-Ling Zhang[1], Xian-Zhong Zheng[1], Bin Li[1], Wen-Tao Luo[34], Wei Liu[1], Jian Wang[38,33], Hong-Fei Zhang[38], Hao Liu[38], Jie Gao[38], Ming Liang[39], Hai-Ren Wang[1], Da-Zhi Yao[1], Jing-Quan Cheng[1], Wen Zhao[4,7], and Zi-Gao Dai[4]

[1] Purple Mountain Observatory, Chinese Academy of Sciences, Nanjing 210023, People's Republic of China; jjgeng@pmo.ac.cn, jzyan@pmo.ac.cn
[2] INAF—Osservatorio Astronomico di Brera, Via E. Bianchi 46, 23807 Merate, LC, Italy; huyoudong072@hotmail.com
[3] Instituto de Astrofísica de Andalucía (IAA-CSIC), Glorieta de la Astronomía s/n, E-18008, Granada, Spain
[4] School of Astronomy and Space Sciences, University of Science and Technology of China, Hefei 230026, People's Republic of China
[5] Unidad Asociada al CSIC Departamento de Ingeniería de Sistemas y Automática, Escuela de Ingenierías, Universidad de Málaga, C. Dr. Ortiz Ramos s/n, 29071 Málaga, Spain
[6] School of Astronomy and Space Science, Nanjing University, Nanjing 210023, People's Republic of China
[7] National Astronomical Observatory of Japan, National Institutes of Natural Sciences, Tokyo 181-8588, Japan
[8] CAS Key Laboratory for Research in Galaxies and Cosmology, Department of Astronomy, University of Science and Technology of China, Hefei, 230026, People's Republic of China
[9] Petro Mohyla Black Sea National University, Mykolaiv 54000, Ukraine
[10] Mykolaiv Astronomical Observatory, Mykolaiv 54030, Ukraine
[11] Department of Algebra, Geometry and Topology, Facultad de Ciencias, Universidad de Málaga, Boulevard Luis Pasteur, sn, E-29071, Málaga, Spain
[12] Servicios Centrales de Investigación, Universidad de Málaga, Boulevard Luis Pasteur, s/n, E-29071, Málaga, Spain
[13] Yunnan Observatories, Chinese Academy of Sciences, Kunming 650216, People's Republic of China
[14] Aryabhatta Research Institute of Observational Sciences (ARIES), Manora Peak, Nainital-263002, India
[15] Instituto de Astronomía, Universidad Nacional Autónoma de México, Carr. Tijuana-Ensenada km.107, 22860 Ensenada, B.C., México
[16] Instituto de Astronomía, Universidad Nacional Autónoma de México, Apdo Postal 70-264, Cd. Universitaria, 04510 México DF, México
[17] Sociedad Malagueña de Astronomía, República Argentina 2, 29071 Málaga, Spain
[18] Department of Physics, Sungkyunkwan University, Seobu-ro 2066, Suwon, 16419, Republic of Korea
[19] Agency for Defense Development, Daejeon 34060, Republic of Korea
[20] Department of Physics, University of the Free State, P.O. Box 339, Bloemfontein 930, South Africa
[21] School of Physics, O'Brien Centre for Science North, University College Dublin, Belfield, Dublin 4, Ireland
[22] Key Laboratory of Modern Astronomy and Astrophysics (Nanjing University), Ministry of Education, Nanjing 210093, People's Republic of China
[23] Millennium Nucleus on Transversal Research and Technology to Explore Supermassive Black Holes (TITANS), Chile
[24] Millennium Institute of Astrophysics (MAS), Nuncio Monseñor Sótero Sanz 100, Providencia, Santiago, Chile
[25] Instituto de Física y Astronomía, Facultad de Ciencias, Universidad de Valparaíso, Gran Bretana 1111, Playa Ancha, Valparaíso, Chile
[26] Swedish Institute of Space Physics (IRF), Bengt Hultqvists väg 1, 981 92 Kiruna, Sweden
[27] University of Helsinki, Faculty of Science, Gustav Hällströmin katu 2, FI-00014, Finland
[28] Institute of Physics and Technology, Ural Federal University, Mira str. 19, 620002 Ekaterinburg, Russia
[29] INAF, Osservatorio di Astrofisica e Scienza dello Spazio di Bologna, via Piero Gobetti 93/3, 40024, Bologna, Italy
[30] Università degli Studi dell'Insubria, Dipartimento di Scienza e Alta Tecnologia, via Valleggio 11, I-22100 Como, Italy
[31] INAF—Osservatorio Astronomico di Roma, Via di Frascati 33, 00040 Monte Porzio Catone, RM, Italy
[32] University of Messina, MIFT Department, Via F. S. D'Alcontres 31, Papardo, 98166 Messina, Italy
[33] Institute of Deep Space Sciences, Deep Space Exploration Laboratory, Hefei 230026, People's Republic of China
[34] Department of Physics and Astronomy, Texas A&M University, College Station, TX 77843-4242, USA
[35] George P. and Cynthia Woods Mitchell Institute for Fundamental Physics and Astronomy, Texas A&M University, College Station, TX 77843-4242, USA
[36] McWilliams Center for Cosmology, Department of Physics, Carnegie Mellon University, 5000 Forbes Ave., Pittsburgh, PA 15213, USA
[37] Institute of Optics and Electronics, Chinese Academy of Sciences, Chengdu 610209, People's Republic of China
[38] State Key Laboratory of Particle Detection and Electronics, University of Science and Technology of China, Hefei 230026, People's Republic of China
[39] National Optical Astronomy Observatory (NSF's National Optical-Infrared Astronomy Research Laboratory), 950 N Cherry Ave., Tucson, AZ 85726, USA

Received 2024 September 1; revised 2024 October 7; accepted 2024 October 8; published 2024 November 21

Abstract

Thanks to the rapidly increasing time-domain facilities, we are entering a golden era of research on gamma-ray bursts (GRBs). In this Letter, we report our observations of GRB 240529A with the Burst Optical Observer and Transient Exploring System, the 1.5 m telescope at Observatorio de Sierra Nevada, the 2.5 m Wide Field Survey Telescope of China, the Large Binocular Telescope, and the Telescopio Nazionale Galileo. The prompt emission of

GRB 240529A shows two comparable energetic episodes separated by a quiescence time of roughly 400 s. Combining all available data on the GRB Coordinates Network, we reveal the simultaneous apparent X-ray plateau and optical rebrightening around 10^3–10^4 s after the burst. Rather than the energy injection from the magnetar as widely invoked for similar GRBs, the multiwavelength emissions could be better explained as two shocks launched from the central engine separately. The optical peak time and our numerical modeling suggest that the initial bulk Lorentz factor of the later shock is roughly 50, which indicates that the later jet should be accretion driven and have a higher mass loading than a typical one. The quiescence time between the two prompt emission episodes may be caused by the transition between different accretion states of a central magnetar or black hole, or the fallback accretion process. A sample of similar bursts with multiple emission episodes in the prompt phase and sufficient follow-up could help to probe the underlying physics of GRB central engines.

Unified Astronomy Thesaurus concepts: Gamma-ray bursts (629); High energy astrophysics (739); Non-thermal radiation sources (1119); Optical observation (1169); Relativistic jets (1390)

Materials only available in the online version of record: machine-readable table

1. Introduction

Gamma-ray bursts (GRBs) are the most powerful explosions in the Universe. They are classified into short/long GRBs according to their duration in gamma rays or the collapsar-/merger-origin GRBs, depending on the progenitor that generated the explosion (P. Kumar & B. Zhang 2015; B. Zhang 2018; A. J. Castro-Tirado et al. 2024). The prompt emission of GRBs is thought to result from the internal dissipation of the outflow launched from the central engine (e.g., M. J. Rees & P. Mészáros 1994), while the subsequent multiwavelength afterglows are the synchrotron radiation produced by the propagation of shocks in the circumburst medium (T. Piran 1999; R. Sari & T. Piran 1999). X-ray observations by the Neil Gehrels *Swift* Observatory (hereafter Swift; N. Gehrels et al. 2004; D. N. Burrows et al. 2005) revealed diverse light curves after the burst, including features like steep decay, flares, plateau, and normal decay (B. Zhang et al. 2006; C.-H. Tang et al. 2019). Meanwhile, some GRBs exhibit rebrightenings in the optical bands (e.g., D. A. Kann et al. 2024). These are characteristics that deviate from the expectations of the standard model, i.e., a simple outgoing blast wave that gives synchrotron radiations (e.g., R. D. Blandford & C. F. McKee 1976; R. Sari & T. Piran 1999; Y. F. Huang et al. 2000; X.-G. Wang et al. 2015), therefore providing valuable opportunities to advance our understanding of GRBs' central engines.

In this Letter, we report our observations and analyses on GRB 240529A, a recently discovered GRB with simultaneous apparent X-ray plateau and optical rebrightening. The rapid follow-ups by space-based and ground-based facilities globally result in a unique story in the GRB museum. This Letter is organized as follows: In Section 2, we describe the observations and data analysis process. Multiwavelength modeling is present in Section 3, and relevant implications and constraints are discussed in Sections 4 and 5. We summarize our results in Section 6.

2. Observations

GRB 240529A is a long GRB, which first triggered the Swift Burst Alert Telescope (BAT; S. D. Barthelmy et al. 2005; R. A. J. Eyles-Ferris et al. 2024) on 2024 May 29, 02:58:31 (UT), and was successively followed in the X-ray band by the X-ray Telescope (XRT; D. N. Burrows et al. 2004; R. A. J. Eyles-Ferris et al. 2024) and the optical band by the Ultra-Violet/Optical Telescope (P. W. A. Roming et al. 2005; S. P. R. Shilling et al. 2024). The refined BAT ground-calculated position is R.A., decl. = 335°.341, 51°.557 (J2000) (C. B. Markwardt et al. 2024). The AstroSat satellite (J. Joshi et al. 2024), the Hard X-ray Modulation Telescope (W. Tan et al. 2024), and the Interplanetary Network (A. S. Kozyrev et al. 2024) soon confirmed this detection. It was found that this burst consists of two separate multipeaked emission episodes by Konus-Wind (D. Svinkin et al. 2024), among which the first episode starts at a gap time of $T_{\rm gap} \sim 400$ s earlier than the second one detected by Swift. These two comparable energetic burst episodes with a clear quiescence time seem rare in the literature.

Multiwavelength follow-ups have been carried out subsequently, ranging from X-rays (J. D. Gropp et al. 2024) to the optical (G. Lim et al. 2024; D. Dutton et al. 2024; S. Y. Fu et al. 2024; Y. D. Hu et al. 2024; A. Kumar et al. 2024; V. Lipunov et al. 2024; G. Mo et al. 2024; T. Mohan et al. 2024; A. S. Moskvitin et al. 2024; M. Odeh et al. 2024; N. Pankov et al. 2024; I. Perez-Garcia et al. 2024; A. K. Ror et al. 2024; J. Vinko et al. 2024) and radio bands (L. Rhodes et al. 2024). Its redshift is identified as $z = 2.695$ using OSIRIS + at the 10.4 m Gran Telescopio Canarias telescope at the Roque de los Muchachos Observatory (A. de Ugarte Postigo et al. 2024). This gives an equivalent isotropic energy of $\simeq 10^{54}$ erg for each episode (D. Svinkin et al. 2024).

2.1. Ground Observations

The Burst Optical Observer and Transient Exploring System (BOOTES; A. J. Castro-Tirado 2023; Y.-D. Hu et al. 2023) network observed the afterglow of GRB 240529A with three telescopes for consecutive observations in clear filters: BOOTES-6 (Dolores Pérez-Ramírez Telescope) 0.6 m robotic telescope at Boyden Observatory, South Africa; BOOTES-5 (Javier Gorosabel Telescope) 0.6 m telescope at Observatorio Astronómico Nacional en la Sierra de San Pedro Mártir, Mexico; and BOOTES-7 telescope at San Pedro de Atacama Space Observatory, Chile. The BOOTES-6 telescope observed the GRB 240529A starting on 2024 May 29, 03:05 UT (about 419 s after the BAT trigger).

We have triggered the 1.5 m telescope at Observatorio Sierra Nevada (OSN; Granada, Spain) for the afterglow observations in *R* and *Ic* bands since 2024 June 1, at 01:06 UT (~2.9 days postburst). We also initiated a follow-up campaign with the 2.5 m Wide Field Survey Telescope (WFST) in the *g* and *r* bands separately after midnight of May 29 and on May 30. WFST is a newly established photometric survey facility equipped with a 2.5 m diameter primary mirror installed near the summit of Saishiteng Mountain in northwestern China (T. Wang et al. 2023).

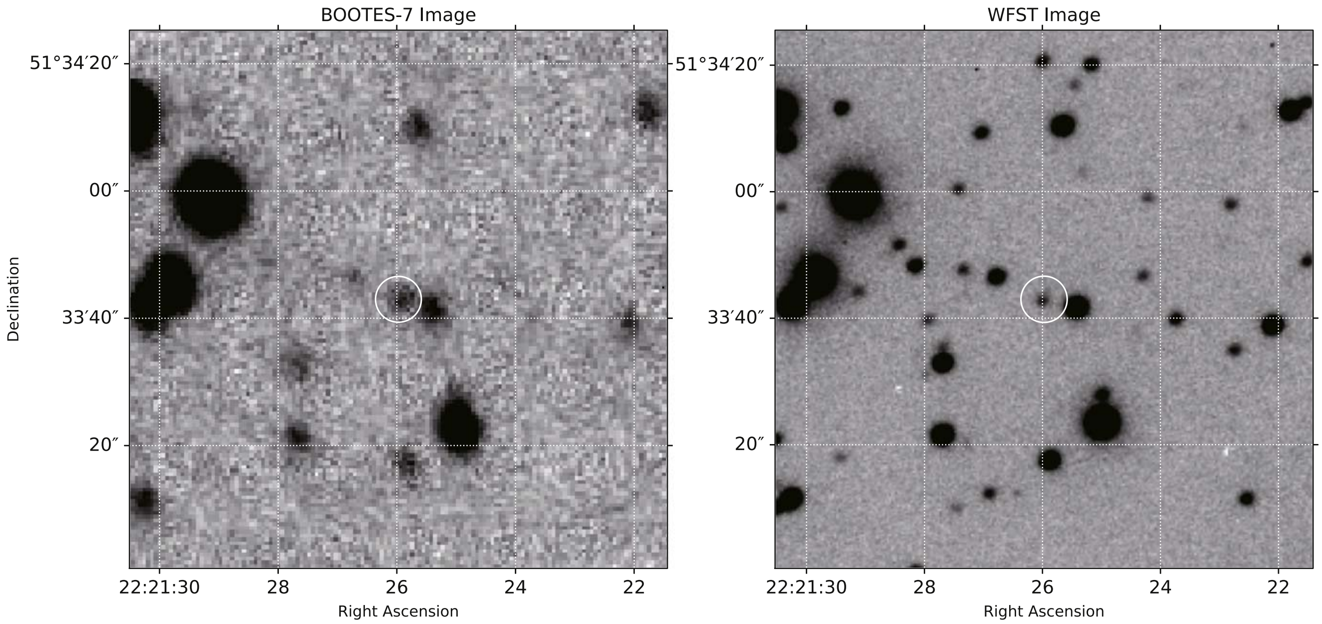

Figure 1. The left image exhibits the BOOTES-7 image observed at 09:44:40 on 2024 May 29 with a 60 s exposure and a magnitude limit of 18.3 mag in the *clear* filter. The right image exhibits the WFST image observed in the *g* band at 18:29:01 on 2024 May 29 with a 180 s exposure and a magnitude limit of 22.1. Note that in both images, the circle indicates the position of GRB 240529A, with north registered as up.

Late-time observations of the field were performed with the Large Binocular Telescope (LBT) using the twin Large Binocular Cameras instruments equipped with the UV filter $U_{\rm spec}$ and the Sloan filters $g'r'i'z'$ on 2024 June 5 (A. Rossi et al. 2024) at the midtime 09:45 UT (7.28 days after the burst trigger). A second deep epoch was obtained in the $r'i'$ filters on 2024 June 12 at the midtime of 08:55 UT (14.25 days after the burst). Additionally, on the same night, *J*-band imaging was also obtained (20:30 UT, ∼14.3 days after the trigger).

2.2. Data Reduction

The basic data reduction followed the standard CCDPROC procedure (M. W. Craig et al. 2015), and the astrometric solution was corrected with the Gaia-DR2 catalog (D. Lang et al. 2010; L. Lindegren et al. 2018). The astrometric solutions for WFST used a triangle match method (Y.-D. Ping 2024, in preparation) with the Gaia-DR2 catalog.

For the data from the BOOTES network, we registered all observation images into the same projection using the SWarp procedure (E. Bertin 2010). We performed a forced photometry method with the Source Extractor (E. Bertin & S. Arnouts 1996) with point-spread function (PSF) results generated by PSFEx (E. Bertin 2013). The observation of BOOTES networks was using the *clear* filter, so we calibrated the observation results to *G* magnitude in the Gaia-DR2 catalog (Gaia Collaboration et al. 2018) as magnitude references.

The photometry results for the WFST data were generated by a pipeline with the PSF photometry using the Source Extractor with the PSF results generated by PSFEx. The magnitude calibration of WFST observational data was calibrated against the Pan-STARRS DR1 catalog (K. C. Chambers et al. 2016). Representative images of GRB 240529A observed by BOOTES and WFST are shown in Figure 1.

The afterglow of GRB 240529A in the photometry images of the OSN telescope was very faint. We took images with the OSN telescope on August 10 as the reference images for image subtractions. We registered all the images to the same projection with SWarp and performed image subtractions with the Saccadic Fast Fourier Transform package (L. Hu et al. 2022). The photometry results were generated by forced photometry with photutils (L. Bradley et al. 2024) on the difference images. The observational results in the *R* and *Ic* bands for OSN observations were calibrated with the Pan-STARRS DR1 catalog and their bandpass transformations (J. L. Tonry et al. 2012).

All LBT data were reduced using the data reduction pipeline developed at INAF—Osservatorio Astronomico di Roma (A. Fontana et al. 2014), which includes bias subtraction and flat-fielding, bad-pixel and cosmic-ray masking, astrometric calibration, and coaddition. The LBT telescope provided very deep images with magnitude limits reaching 25.5 mag in *i* band from the coadded image. Since the point source of GRB 240529A is clearly detected in the LBT image, we performed PSF photometry using the stand-alone DAOPHOT package (P. B. Stetson 1987) on these coadded images. The observational results in the *g*, *r*, *i*, and *z* bands for LBT observations were calibrated against the Pan-STARRS DR1 catalog. We cannot identify any emission from an extended source, i.e., host galaxy, at the location of the afterglow. Indeed, in the late images, we identify the possible host galaxy to be offset (between 1″ and 2″, ≈8–16 kpc) from the afterglow (R.A. (J2000) = $22^{\rm h}21^{\rm m}25\overset{\rm s}{.}94$, decl. (J2000) = $+51°33'40\overset{\prime\prime}{.}6$) from the LBT image; thus, we will not consider the host contribution in our modeling of the light curve.

The TNG image was reduced using the jitter task from the ESO eclipse package[40] (N. Devillard 1997). Photometric measurements were obtained through both aperture photometry and PSF-matched photometry with the DAOPHOT package within IRAF (D. Tody 1986), which were calibrated against nearby reference stars listed in the 2MASS catalog (M. F. Skrutskie et al. 2006).

All the photometry results are shown in Table 1.

[40] https://www.eso.org/sci/software/eclipse/

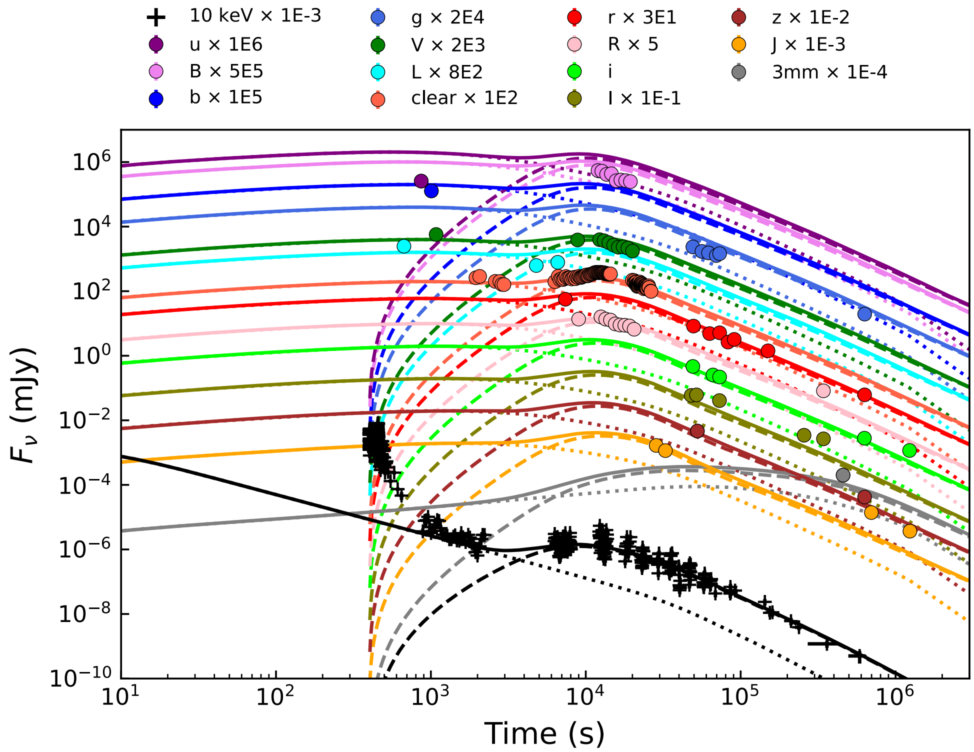

Figure 2. Modeling the multiwavelength afterglow of GRB 240529A with the two external shocks. The dotted and dashed lines represent emissions from the former and the later shocks, respectively, and the the solid lines are the sum of them. The X-ray data are taken from the Swift/XRT website (http://www.swift.ac.uk/xrt_curves/01231488/). The optical data are taken from Section 2 and GCN circulars (C. Adami et al. 2024; J. An et al. 2024; A. de Ugarte Postigo et al. 2024; D. Dutton et al. 2024; S. Y. Fu et al. 2024; G. Lim et al. 2024; G. Mo et al. 2024; T. Mohan et al. 2024; M. Niwano et al. 2024; M. Odeh et al. 2024; N. Pankov et al. 2024; A. K. Ror et al. 2024; A. Rossi et al. 2024; J. Vinko et al. 2024). The radio data are taken from L. Rhodes et al. (2024). Note that the prompt emission and the steep decay of the later burst are not used in the fitting. The optical data have been corrected for Galactic extinction of $E(B-V)=0.29$ mag (E. F. Schlafly & D. P. Finkbeiner 2011). The excess of the modeling flux at the short wavelengths hints at the potential extinction of the host galaxy.

Table 1
All Photometry of GRB 240529A

$T-T_0$ (s)	$\sigma_{\rm T}$ (s)	MJD (days)	$\sigma_{\rm MJD}$ (days)	Mag	$\sigma_{\rm mag}$	Filter	Telescope
1552.42	60.00	60459.141938	0.000700	16.13	0.10	clear	BOOTES-6
55830.00	180.00	60459.770150	0.002083	20.11	0.03	g	WFST
256226.16	3929.16	60462.089550	0.045500	20.59	0.09	I	OSNT150
629256.50	843.00	60466.407031	0.009800	23.36	0.09	i	LBT
697453.00	3459.00	60467.196343	0.040035	21.30	0.34	J	TNG
...	...	...	...	...	...	...	...

Note. Magnitudes are only calibrated with reference catalogs described in Section 2, without the extinction corrections in the Milky Way or GRB host galaxy.

(This table is available in its entirety in machine-readable form in the online article.)

3. Modeling

Combining all the available data, we show the multiwavelength afterglow emissions of GRB 240529A in Figure 2. During the prompt phase, the released isotropic gamma-ray energy of each episode is $\simeq 10^{54}$ erg (D. Svinkin et al. 2024). Rather than a power-law decay in normal bursts, optical afterglows show rebrightenings with a peak time of $\simeq 1.2 \times 10^4$ s in GRB 240529A, accompanied by an apparent X-ray plateau. The long-term monitoring of XRT indicates that the temporal index changes from -1.76 ± 0.03 to -2.74 ± 0.21 at $\sim 10^5$ s, which may be a result of the jet beaming break (T. Piran 2000). However, no significant simultaneous break is present in optical bands due to insufficient observation sampling around this time. In the following, two possible scenarios are explored to understand the characteristics of GRB 240529A.

3.1. The Magnetar Scenario

Energy injection processes (Z. G. Dai & T. Lu 1998a, 1998b; Y.-Z. Fan & D. Xu 2006; J. J. Geng et al. 2013; H. van Eerten 2014) or the refreshing of the forward shock (FS) by late-arriving shells (B. Zhang & P. Mészáros 2001) are often invoked to explain the production of an X-ray plateau. On the other hand, it has been suggested that the central engines of some GRBs are newly born magnetars, from which a wind of Poynting flux (Z. G. Dai & T. Lu 1998b; B. Zhang et al. 2006) or electron–positron pairs could inject into the FS and result in an X-ray plateau (Z. G. Dai 2004; Y. W. Yu & Z. G. Dai 2007; Y. W. Yu et al. 2007). This magnetar model has successfully been applied in explaining the simultaneous X-ray plateau and the optical rebrightening in some GRB afterglows (J. J. Geng et al. 2016; J.-J. Geng et al. 2018a). However, we realize that this scenario

Table 2
Parameters Used in the Modeling of the Afterglow of GRB 240529A

Parameters	Former Shock[a]	Later Shock
$E_{\rm K,iso}$ (10^{54} erg)	1.0	$5.0^{-0.001}_{+0.001}$
Γ_0	800	$43.6^{+0.1}_{-0.1}$
$\theta_{\rm j}$ (rad)	0.05	$0.03^{+0.001}_{-0.001}$
p	2.4	$2.05^{+0.001}_{-0.001}$
$\xi_{\rm e}$	0.1	$0.24^{+0.003}_{-0.004}$
ξ_B	2.0×10^{-4}	$1.6^{+0.04}_{-0.04} \times 10^{-4}$
n (cm^{-3})	7.0	$10.0^{+0.02}_{-0.05}$

Note.
[a] It is hard to constrain the parameters of the former shock strictly.

requires an unusually high stellar spin in the case of GRB 240529A, as estimated in the following paragraph, unless a Poynting-flux-dominated wind or an electron–positron-pair-dominated wind that is available for energy injection is beamed in a jet.

The wind luminosity from the rotating magnetosphere of the magnetar is (e.g., S. L. Shapiro & S. A. Teukolsky 1983; R. X. Xu & G. J. Qiao 2001; I. Contopoulos & A. Spitkovsky 2006)

$$L_{\rm w} = 9.6 \times 10^{46} B_{\rm NS,14}^2 R_{\rm NS,6}^6 P_{0,-3}^{-4} \left(1 + \frac{t_{\rm obs}}{T_{\rm sd}}\right)^{-2} \ {\rm erg\ s^{-1}}, \quad (1)$$

where $B_{\rm NS}$ is the strength of the surface magnetic field of the magnetar, $R_{\rm NS}$ is the radius, P_0 is the initial spin period, $T_{\rm sd} \simeq 2 \times 10^5 (1 + z) I_{45} B_{\rm NS,14}^{-2} R_{\rm NS,6}^{-6} P_{0,-3}^2$ s is the spin-down timescale of the magnetar, and I is its moment of inertia. The convention $Q_x = Q/10^x$ in centimeter gram second units is adopted hereafter. If we attributed the X-ray luminosity near the end of the plateau to the dissipation of the magnetar wind with an efficiency of η, i.e., $L_{\rm X} \simeq \eta L_{\rm w}(T_{\rm sd})$, one can obtain

$$P_0 \leqslant 0.1 \left(\frac{\eta}{0.1}\right)^{1/2} \left(\frac{I}{10^{45}\ {\rm g\ cm^2}}\right)^{1/2} \times \left(\frac{L_{\rm X}}{10^{49}\ {\rm erg\ s^{-1}}}\right)^{-1/2} \left(\frac{T_{\rm sd}}{10^4\ {\rm s}}\right)^{-1/2} {\rm ms}, \quad (2)$$

which requires a newborn submillisecond magnetar for GRB 240529A with $L_{\rm X} = 4\pi D_{\rm L}^2 F_{\rm X}/(1 + z)^{1-\beta_{\rm X}} \simeq 2 \times 10^{49}$ erg s^{-1} and $T_{\rm sd} \simeq 10^4$ s as inferred from the X-ray data. Here, an observed flux of $F_{\rm X} \simeq 3 \times 10^{-10}$ erg cm^{-2} s^{-1} and a spectral index of $\beta_{\rm X} \simeq 1.2$ by the XRT is used. Such a rapidly rotating neutron star is outside of the magnetars associated with GRBs with plateaus (G. Stratta et al. 2018) and beyond the prediction of any equation of state for dense nuclear matter. However, it could be a strange quark star (J. A. Frieman & A. V. Olinto 1989). This is because the gravitational-radiation-driven r-mode instability of a rapidly spinning star is highly suppressed due to a large bulk viscosity associated with the nonleptonic weak interaction among quarks, and thus a newborn strange quark star can rotate at a submillisecond period (Z. G. Dai et al. 2016).

3.2. The Two-shock Scenario

Considering that there are two energetic emission episodes in the prompt phase, it is reasonable to suppose that each episode would drive an FS into the circumburst environment and the observed flux is the superposition of the emission from these two shocks. Energy extraction processes directly from the central engine do not suffer from the energy budget issue discussed in Section 3.1. In this scenario, the early observed decaying optical afterglow is contributed by the former shock, while the optical rebrightening is due to the onset of the emission from the later shock. Since the emission of the former shock is obscured by that of the later shock for $t_{\rm obs} \geqslant 5 \times 10^3$ s, it is difficult to sufficiently constrain relevant parameters of the former shock. The parameters of the former shock are chosen to interpret the early decaying optical afterglow within $\sim 3 \times 10^3$ s (i.e., the coasting phase is too short) and to ensure that the X-ray afterglow does not exceed the observed flux of the second prompt episode. The scarcity of data and the strong degeneracy among parameters render these parameter values solely for reference purposes. As the afterglow temporal indices of one shock usually get steeper with time, it is reasonable to assume that the emission of the former shock is much fainter than that of the later shock. Therefore, how the early emission is modeled has little influence on fitting to the rest of the data. Hence, we mainly focus on the properties of the later shock below. Assuming that the initial Lorentz factor and the isotropic kinetic energy of the later shock are Γ_0 and $E_{\rm K,iso}$, the peak time of the optical rebrightening corresponds to the end of the coasting phase of the blast wave in the standard GRB shock model (R. D. Blandford & C. F. McKee 1976; R. Sari & T. Piran 1999), i.e.,

$$t_{\rm peak} \simeq 10^4 \left(\frac{E_{\rm K,iso}}{10^{54}\ {\rm erg}}\right)^{1/3} \left(\frac{n}{1\ {\rm cm^{-3}}}\right)^{-1/3} \left(\frac{\Gamma_0}{50}\right)^{-8/3} {\rm s}, \quad (3)$$

where n is the number density of the ambient medium experienced by the later shock. The relatively long peak time of $\simeq 10^4$ s of GRB 240529A indicates that Γ_0 of the later shock should be significantly smaller than the typical value of ~ 300 (G. Ghirlanda et al. 2018).

Detailed numerical calculations to fit the multiwavelength data are performed to demonstrate the consistency of this scenario. The generical dynamical equations (Y. F. Huang et al. 1999, 2000; A. Pe'er 2012) incorporating the jet sideways expansion (J. Granot & T. Piran 2012) are adopted to describe the jet dynamics. We then solve the continuity equation of electrons accelerated by the FS in the energy space, from which multiwavelength afterglows are derived (J.-J. Geng et al. 2018b; H.-X. Gao et al. 2024). The "thermal" electrons due to the inefficient shock heating are included in our calculations (D. Giannios & A. Spitkovsky 2009; H.-X. Gao et al. 2024). Specifically, the ratio of the nonthermal electron energy to the whole shocked electron energy δ is taken as 0.8. Seven parameters, i.e., $E_{\rm K,iso}$, Γ_0, the half-opening angle of the jet $\theta_{\rm j}$, the accelerated electron spectral index p, the equipartition parameters for shocked electrons $\xi_{\rm e}$ and magnetic fields ξ_B, and the medium density number n are left free for each shock. Parameters of the former shock are chosen after several trials by hand. In contrast, parameters of the later shock are constrained by embedding our numerical module into the prevailing Markov Chain Monte Carlo Ensemble sampler called emcee (D. Foreman-Mackey et al. 2013), as in our previous works (J. J. Geng et al. 2016; F. Xu et al. 2022). The posteriors are listed in Table 2 and Figure 3, whose derived initial bulk Lorentz factor of $\Gamma_0 = 43.6^{+0.1}_{-0.1}$ is consistent with the analytical analysis above. Figure 2 shows that the observed afterglows are well explained by those predicted by the two-

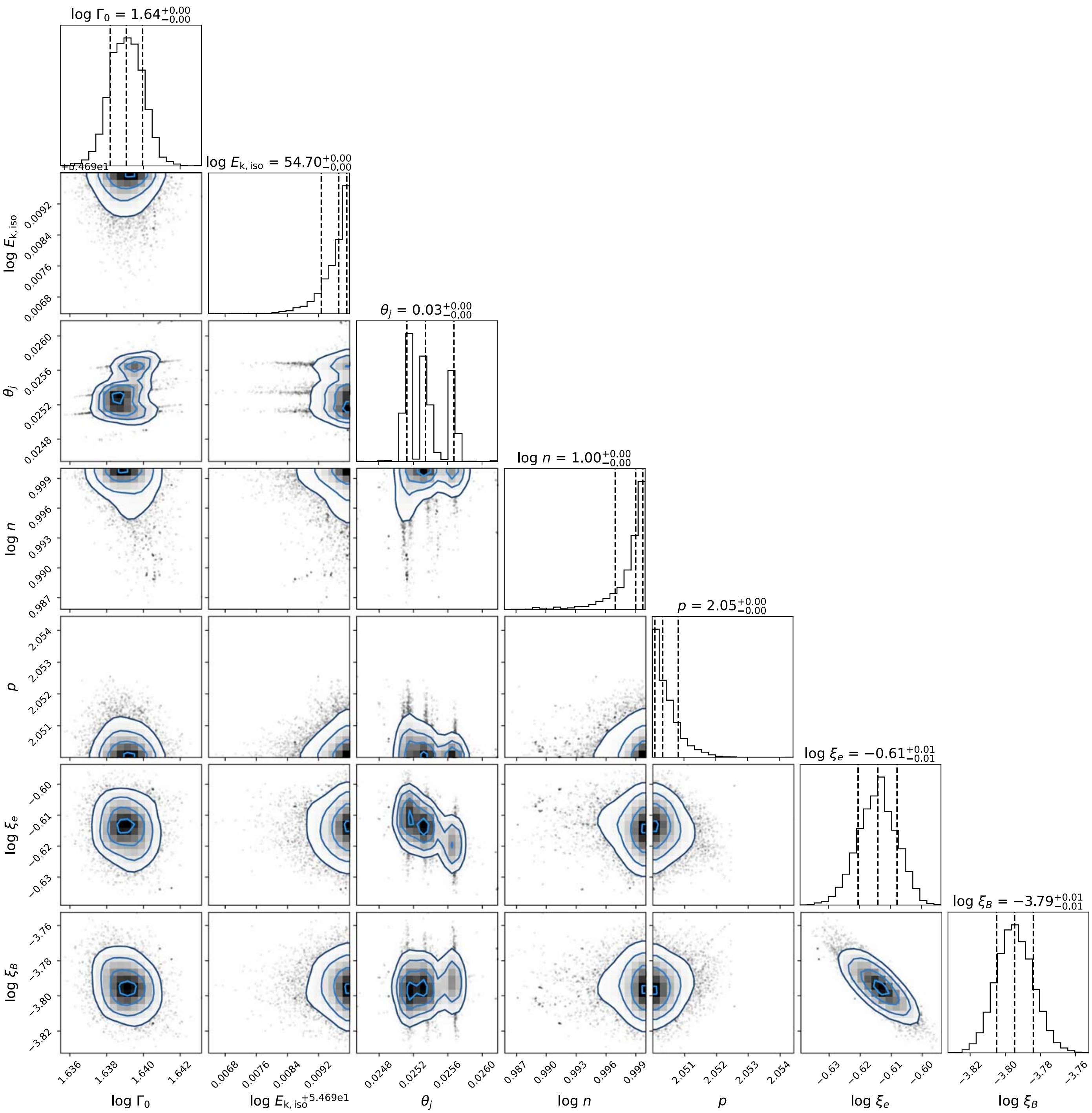

Figure 3. The corner plot of the fitting result in Figure 2. It shows all the one- and two-dimensional projections of the posterior probability distributions of seven model parameters listed in Table 2. The one-dimensional histograms are marginal posterior distributions of these parameters, in which the vertical dashed lines indicate the 16th, 50th, and 84th percentiles of the samples, respectively.

shock scenario. Since the highest photon energy of $\simeq$3 MeV announced by Konus-Wind (D. Svinkin et al. 2024) is less than the critical value of $\Gamma_0 m_e c^2/(1+z) \simeq 6$ MeV, the photons would not suffer from the annihilation during the prompt phase. Detailed spectral analyses may give a more robust low limit for allowed values of Γ_0. Due to the degeneracy between $E_{\mathrm{K,iso}}$ and n, and the uncertainty of radiation efficiency during the prompt phase, $E_{\mathrm{K,iso}}$ always tends to be a large value, i.e., the upper boundary of the priors. Note that the ambient number density for the two shocks launched subsequently is not necessarily the same since the leading one would modify the environment.

The observational flux density of the J band exceeds our afterglow modeling at the late time around 10^6 s (see Figure 2). This exceeding flux corresponds to a component with a luminosity level of 10^{44} erg s^{-1} in the ultraviolet band at the rest frame, which could be emissions from the shock breakout in a supernova (S. Gezari et al. 2015), a potential superluminous supernova (M. R. Drout et al. 2014), or other underlying sources. Its exact origin is highly uncertain and out of the scope of this Letter.

4. Discussion

As the two-shock scenario could well explain the multiwavelength emission of the GRB 240529A, the underlying physics to launch two energetic jets separately from the central engine remains puzzling. Three possible origins are discussed here.

First, if the central engine is a magnetar, the bursting phase and the quiescence time may be interpreted as the transition between the accretion and propeller phases, regulated by the ordering of the magnetospheric radius and the corotation radius (Z. G. Dai & R.-Y. Liu 2012; S. Dall'Osso et al. 2023). The magnetospheric radius (a fraction of the Alfvén radius) is $r_{\rm m} \propto \mu^{4/7}\dot{m}^{-2/7}$, and the corotation radius writes as $r_{\rm co} = (GMP^2/4\pi^2)^{1/3}$, where μ is the magnetic moment and $\dot{m}$ is the mass accretion rate. The infant magnetar may take time to amplify its surface magnetic field and establish a relatively stable configuration (R. Raynaud et al. 2020), during which the accretion would occur and produce the first emission episode. When the magnetic field becomes strong enough, the emission ends as the system enters into the propeller regime ($r_{\rm m} \geqslant r_{\rm co}$). After a period of inactivity, the accretion will start again once the magnetar spin slows down to get into the accretion regime ($r_{\rm m} \simeq r_{\rm co}$) and hence will produce the second emission episode. Assuming the burst luminosity to be $\propto \dot{m}c^2$, the quiescence time between two burst episodes gives

$$T_{\rm sd} \leqslant \frac{T_{\rm gap}}{(\bar{L}_1/\bar{L}_2)^{6/7} - 1} \equiv Y, \tag{4}$$

where $\bar{L}_1$ and $\bar{L}_2$ are the average luminosity of the former and later bursts, respectively. Taking $\bar{L}_1/\bar{L}_2 \simeq 3$ and $T_{\rm gap} \simeq 400$ s, it further constrains the surface magnetic field strength to be

$$B_{\rm NS} \geqslant 6 \times 10^{15}\left(\frac{Y}{130}\right)^{-1/2}\left(\frac{I}{10^{45}\ {\rm g\ cm^2}}\right)^{1/2} \times \left(\frac{P_0}{1\ {\rm ms}}\right)\left(\frac{R_{\rm NS}}{10^6\ {\rm cm}}\right)^{-3} {\rm G}, \tag{5}$$

which is consistent with the magnetar assumption.

Second, if the central engine is a rotating black hole (BH), it is suggested that relativistic jets could be launched from the magnetically arrested disk (A. Tchekhovskoy et al. 2011). In this scenario, the quiescence time longer than 10 s may correspond to the time in which the disk undergoes the interchange instability and the flux diffuses out into the disk (N. M. Lloyd-Ronning et al. 2016). The activity may restart after a viscosity timescale of $\tau_{\rm vis}$. Under a simple Shakura–Sunyaev prescription of the disk around a BH with a mass of $M_{\rm BH}$, we have (e.g., N. M. Lloyd-Ronning et al. 2016; W.-H. Lei et al. 2017; T. Liu et al. 2017)

$$\tau_{\rm vis} \simeq 1\left(\frac{\alpha}{0.1}\right)^{-1}\left(\frac{H/R}{0.3}\right)^{-2}\left(\frac{R}{30\ R_{\rm g}}\right)^{3/2}\left(\frac{M_{\rm BH}}{5\ M_\odot}\right) {\rm s}, \tag{6}$$

where α is the viscosity parameter, H/R is the ratio of disk height H to radius R, $R_{\rm g}$ is the Schwarzschild radius, and $M_\odot$ is the solar mass. The relatively longer $T_{\rm gap}$ here may indicate that the H/R is somehow smaller. Also, other reasons like fallback debris (J. K. Cannizzo et al. 1990; J. K. Cannizzo & N. Gehrels 2009; W. H. Lee et al. 2009) can be invoked to explain for the second energetic burst.

At last, the central engine may be a rapidly rotating supramassive neutron star initially that collapses into a BH later (M. Vietri & L. Stella 1998; H. Falcke & L. Rezzolla 2014; P. D. Lasky et al. 2014; V. Ravi & P. D. Lasky 2014). The collapse time ($\leqslant T_{\rm gap}$) is in the range of $\sim$10–4.4 $\times$ 10^4 s (V. Ravi & P. D. Lasky 2014). In this case, since the disk formation is seemingly unfeasible after the collapse of an isolated neutron star (B. Margalit et al. 2015), additional fallback materials from the progenitor are still required to produce the second burst.

All these possible mechanisms for the long-standing period between the two prompt episodes are principally consistent with the two-shock scenario for afterglow modeling. The significantly smaller bulk Lorentz factor for the second episode suggests that the baryon loading of the second episode is larger than that of a typical burst, supporting an accretion-driven origin. However, it is hard to tell whether the central engine is a magnetar or a BH without clues on the progenitor star type or other robust evidence directly from the central compact star, a critical issue among most GRBs. On the contrary, the apparent X-ray plateau of GRB 240529A reminds us to be careful when we immediately associate the plateau feature with a central magnetar. Had Konus-Wind not detected the former emission episode, such a misleading conclusion would have occurred.

A single jet could be unstable to kink or sausage instabilities caused by toroidal magnetic fields and produce several luminous knots (e.g., E. T. Meyer et al. 2013; O. Bromberg & A. Tchekhovskoy 2016). These knots may be responsible for different emission episodes at the prompt stage. However, it is not easy for these knots to drive relativistic GRB shock and produce subsequent GRB afterglow emission episodes.

5. Model Applicability and Constraints

We now discuss the application scope of the two-shock scenario in the face of the diversity of GRB prompt emission and afterglows. There are GRBs with two equivalent, well-separated peaks in their prompt emission with no rebrightening in their optical afterglow. This could be due to several reasons. First, the catch-up process of the two shocks would merge them into one blast wave soon if the separation time between two peaks is relatively short and the later shock is moving faster. Moreover, shock parameters like kinetic energy of the later shock may produce an afterglow emission fainter than that of the early shock. In addition, the superposition of the two emission components with either fast- or slow-decaying behavior may not necessarily lead to the rebrightening but a smooth temporal transition only. Hence, it is not easy to identify the afterglow emission of the later shock with confidence from the observations like GRB 240529A.

For GRBs with one main emission episode in the prompt phase and rebrightenings in their optical afterglow, the traditional energy injection scenarios should be preferred only if they do not suffer from the energy budget issue of the central engine (Section 3.1).

6. Conclusions

In this Letter, we report our observations of the recently detected GRB 240529A. Our data show clear optical rebrightening with a peak time of $\simeq$1.2 $\times$ 10^4 s. The information on prompt emission motivates us to interpret the apparent

X-ray plateau and the optical rebrightening of GRB 240529A using the two-shock scenario, rather than the traditional magnetar-wind-injection scenario. The peak time of the optical and X-ray afterglow suggests a relatively smaller initial bulk Lorentz factor of $\Gamma_0 \sim 50$ for the later shock, which is also confirmed by the multiwavelength afterglow modeling using our numerical method (J.-J. Geng et al. 2018b; H.-X. Gao et al. 2024).

The prompt energy and Γ_0 of the second episode do not follow the relationship revealed by other bursts with much earlier peak time (E.-W. Liang et al. 2010; S.-X. Yi et al. 2017). This indicates that the baryon loading of the second episode should be larger than that of typical bursts. This high baryon loading may prefer a neutrino-driven jet from a hyperaccreting BH rather than a magnetically dominated jet (W.-H. Lei et al. 2013). In comparison with the first episode, which could be a cleaner jet by extracting the rotation energy of a central BH (R. D. Blandford & R. L. Znajek 1977), an accretion-driven jet for the second episode could be reasonable if the spin of the BH or the surrounding magnetic field strength decreases significantly after a period of 400 s.

In some GRBs, there is a weak precursor before the main burst with the time gap ranging from $\sim$1 to 10^3 s (D. Burlon et al. 2008). Bursts composed of two comparable main phases like GRB 240529A are unusual. It may be due to the difficulty of identifying possible candidates from bursts with multiple peaks and episodes of different energy intensities in practice (L.-B. Li et al. 2015) or the rarity of the physical mechanisms themselves.

Shock parameters like $E_{\mathrm{K,iso}}$ and n are not well constrained in our fit due to the degeneracy between parameters and the radiation efficiency that is poorly known. Nevertheless, current fitting results show that the radiation efficiency of the first episode is higher than that of the second episode, which is consistent with the change of jet property by the different energy extraction mechanisms mentioned above, i.e., from Poynting-flux dominated (C. Thompson 1994; B. Zhang & H. Yan 2011) to baryon-matter dominated (R. Popham et al. 1999; R. Narayan et al. 2001; W.-M. Gu et al. 2006; W.-H. Lei et al. 2013). As more adequate multiwavelength data from the GeV to the radio band are crucial to narrowing down the parameter space, dedicated follow-up schemes of GRB afterglow are eagerly invoked to advance our understanding of GRBs in the current era.

Our work addresses the significance of analyses in the synergy of the prompt emission and the afterglow emission, which will also be shown in a series of works soon. The two active episodes separated by a quiescence time of $\sim$400 s may be caused by the transition between different accretion states of a central magnetar or BH, or the fallback accretion process. High-cadence multiwavelength monitoring of more similar bursts may shed light on the physics of the central engine and progenitors.

Acknowledgments

We thank the anonymous referee for valuable suggestions and Mao-Kai Hu for useful discussions. This study is partially supported by the National Natural Science Foundation of China (grant Nos. 12273113, 12321003, 12393812, 12393813, and 12025303), the National SKA Program of China (grant Nos. 2020SKA0120302 and 2022SKA0130100), the Strategic Priority Research Program of the Chinese Academy of Sciences (grant No. XDB0550400), and the International Partnership Program of Chinese Academy of Sciences for Grand Challenges (114332KYSB20210018). J.J.G. acknowledges support from the Youth Innovation Promotion Association (2023331). A.J.C.T. acknowledges support from the Spanish Ministry projects PID2020-118491GB-I00 and PID2023-151905OB-I00 and Junta de Andalucia grant P20_010168 and from the Severo Ochoa grant CEX2021-001131-S funded by MCIN/AEI/ 10.13039/501100011033. A.R. and E.M. acknowledge support by PRIN-MIUR 2017 (grant 20179ZF5KS). F.C. acknowledges support from the INAF project Premiale Supporto Arizona & Italia.

M.G. acknowledges the Academy of Finland project No. 325806. The program of development within Priority-2030 is acknowledged for supporting the research at UrFU (04.89). L.H.G. acknowledges funding from ANID programs: FONDECYT Iniciación 11241477, and Millennium Science Initiative Programs NCN2023_002 and ICN12_009. L.H. acknowledges support from Science Foundation Ireland grant 19/FFP/6777. G.G.S. acknowledges support from DGAPA-UNAM PASPA grant. Y.D.H. acknowledges financial support from INAF through the GRAWITA Large Program Grant (ID: 1.05.12.01.04). I.H.P. acknowledges the support from NRF-2017K1A4A3015188 and NRF-2021R1A2B5B03002645. T.R.S. and H.X.G. acknowledge support from Jiangsu Funding Program for Excellent Postdoctoral Talent.

The LBT is an international collaboration of the University of Arizona, Italy (INAF: Istituto Nazionale di Astrofisica), Germany (LBTB: LBT Beteiligungsgesellschaft), The Ohio State University, representing also the University of Minnesota, the University of Virginia, and the University of Notre Dame. The WFST team would like to express their sincere thanks to the staff of the Lenghu observation station.

This work has made use of data from the European Space Agency (ESA) mission Gaia (https://www.cosmos.esa.int/gaia), processed by the Gaia Data Processing and Analysis Consortium (DPAC, https://www.cosmos.esa.int/web/gaia/dpac/consortium). This work made use of Astropy (http://www.astropy.org): a community-developed core Python package and an ecosystem of tools and resources for astronomy (Astropy Collaboration et al. 2013, 2018, 2022).

ORCID iDs

Tian-Rui Sun https://orcid.org/0000-0003-1166-3814
Jin-Jun Geng https://orcid.org/0000-0001-9648-7295
You-Dong Hu https://orcid.org/0000-0002-7400-4608
Xue-Feng Wu https://orcid.org/0000-0002-6299-1263
Alberto J. Castro-Tirado https://orcid.org/0000-0003-2999-3563
Chao Yang https://orcid.org/0009-0006-5171-3723
Yi-Ding Ping https://orcid.org/0000-0002-7529-1792
Chen-Ran Hu https://orcid.org/0000-0002-5238-8997
Fan Xu https://orcid.org/0000-0001-7943-4685
Hao-Xuan Gao https://orcid.org/0000-0001-7892-9790
Ji-An Jiang https://orcid.org/0000-0002-9092-0593
Yan-Tian Zhu https://orcid.org/0009-0009-5585-4728
Yongquan Xue https://orcid.org/0000-0002-1935-8104
Ignacio Pérez-García https://orcid.org/0000-0002-7273-3671
Si-Yu Wu https://orcid.org/0009-0004-7113-8258
Emilio Fernández-García https://orcid.org/0009-0009-4604-9639
María D. Caballero-García https://orcid.org/0000-0001-7920-4564

Rubén Sánchez-Ramírez https://orcid.org/0000-0002-7158-5099
Sergiy Guziy https://orcid.org/0000-0003-2628-6468
Ding-Rong Xiong https://orcid.org/0000-0002-6809-9575
David Hiriart https://orcid.org/0000-0002-4711-7658
William H. Lee https://orcid.org/0000-0002-2467-5673
Il H. Park https://orcid.org/0000-0001-6665-9631
Petrus J. Meintjes https://orcid.org/0000-0001-8890-5418
Hendrik J. van Heerden https://orcid.org/0009-0004-9747-7215
Antonio Martín-Carrillo https://orcid.org/0000-0001-5108-0627
Lorraine Hanlon https://orcid.org/0000-0003-2931-3732
Bin-Bin Zhang https://orcid.org/0000-0003-4111-5958
L. Hernández-García https://orcid.org/0000-0002-8606-6961
Maria Gritsevich https://orcid.org/0000-0003-4268-6277
Andrea Rossi https://orcid.org/0000-0002-8860-6538
Elisabetta Maiorano https://orcid.org/0000-0003-2593-4355
Felice Cusano https://orcid.org/0000-0003-2910-6565
Andrea Melandri https://orcid.org/0000-0002-2810-2143
Massimiliano De Pasquale https://orcid.org/0000-0002-4036-7419
Riccardo Brivio https://orcid.org/0009-0000-0564-7733
Min Fang https://orcid.org/0000-0001-8060-1321
Lu-Lu Fan https://orcid.org/0000-0003-4200-4432
Wei-Da Hu https://orcid.org/0000-0003-3424-3230
Lei Hu https://orcid.org/0000-0001-7201-1938
Xiao-Ling Zhang https://orcid.org/0000-0003-2100-3596
Xian-Zhong Zheng https://orcid.org/0000-0003-3728-9912
Bin Li https://orcid.org/0000-0001-9327-0920
Wen-Tao Luo https://orcid.org/0000-0003-1297-6142
Wei Liu https://orcid.org/0000-0002-2237-3655
Jian Wang https://orcid.org/0000-0003-1617-2002
Hong-Fei Zhang https://orcid.org/0000-0002-1463-9070
Hai-Ren Wang https://orcid.org/0000-0002-4372-0759
Wen Zhao https://orcid.org/0000-0002-1330-2329
Zi-Gao Dai https://orcid.org/0000-0002-7835-8585

References

Adami, C., Basa, S., de Ugarte Postigo, A., et al. 2024, GCN, 36575, 1
An, J., Liu, X., Zhu, Z. P., et al. 2024, GCN, 36734, 1
Astropy Collaboration, Price-Whelan, A. M., Lim, P. L., et al. 2022, ApJ, 935, 167
Astropy Collaboration, Price-Whelan, A. M., Sipőcz, B. M., et al. 2018, AJ, 156, 123
Astropy Collaboration, Robitaille, T. P., Tollerud, E. J., et al. 2013, A&A, 558, A33
Barthelmy, S. D., Barbier, L. M., Cummings, J. R., et al. 2005, SSRv, 120, 143
Bertin, E. 2010, SWarp: Resampling and Co-adding FITS Images Together, Astrophysics Source Code Library, ascl:1010.068
Bertin, E. 2013, PSFEx: Point-Spread Function Extractor, Astrophysics Source Code Library, ascl:1301.001
Bertin, E., & Arnouts, S. 1996, A&AS, 117, 393
Blandford, R. D., & McKee, C. F. 1976, PhFl, 19, 1130
Blandford, R. D., & Znajek, R. L. 1977, MNRAS, 179, 433
Bradley, L., Sipőcz, B., Robitaille, T., et al. 2024, astropy/photutils: v1.12.0, Zenodo, doi:10.5281/zenodo.10967176
Bromberg, O., & Tchekhovskoy, A. 2016, MNRAS, 456, 1739
Burlon, D., Ghirlanda, G., Ghisellini, G., et al. 2008, ApJL, 685, L19
Burrows, D. N., Hill, J. E., Nousek, J. A., et al. 2004, Proc. SPIE, 5165, 201
Burrows, D. N., Hill, J. E., Nousek, J. A., et al. 2005, SSRv, 120, 165
Cannizzo, J. K., & Gehrels, N. 2009, ApJ, 700, 1047
Cannizzo, J. K., Lee, H. M., & Goodman, J. 1990, ApJ, 351, 38
Castro-Tirado, A. J. 2023, NatAs, 7, 1136
Castro-Tirado, A. J., Gupta, R., Pandey, S. B., et al. 2024, A&A, 683, A55
Chambers, K. C., Magnier, E. A., Metcalfe, N., et al. 2016, arXiv:1612.05560
Contopoulos, I., & Spitkovsky, A. 2006, ApJ, 643, 1139
Craig, M. W., Crawford, S. M., Deil, C., et al. 2015, ccdproc: CCD Data Reduction Software, Astrophysics Source Code Library, ascl:1510.007
Dai, Z. G. 2004, ApJ, 606, 1000
Dai, Z. G., & Liu, R.-Y. 2012, ApJ, 759, 58
Dai, Z. G., & Lu, T. 1998a, PhRvL, 81, 4301
Dai, Z. G., & Lu, T. 1998b, A&A, 333, L87
Dai, Z. G., Wang, S. Q., Wang, J. S., Wang, L. J., & Yu, Y. W. 2016, ApJ, 817, 132
Dall'Osso, S., Stratta, G., Perna, R., De Cesare, G., & Stella, L. 2023, ApJL, 949, L32
de Ugarte Postigo, A., Thoene, C. C., Agui Fernandez, J. F., et al. 2024, GCN, 36574, 1
Devillard, N. 1997, Msngr, 87, 19
Drout, M. R., Chornock, R., Soderberg, A. M., et al. 2014, ApJ, 794, 23
Dutton, D., Reichart, D., Haislip, J., et al. 2024, GCN, 36568, 1
Eyles-Ferris, R. A. J., Gupta, R., Lien, A. Y., et al. 2024, GCN, 36556, 1
Falcke, H., & Rezzolla, L. 2014, A&A, 562, A137
Fan, Y.-Z., & Xu, D. 2006, MNRAS, 372, L19
Fontana, A., Dunlop, J. S., Paris, D., et al. 2014, A&A, 570, A11
Foreman-Mackey, D., Conley, A., Meierjurgen Farr, W., et al. 2013, emcee: The MCMC Hammer, Astrophysics Source Code Library, ascl:1303.002
Frieman, J. A., & Olinto, A. V. 1989, Natur, 341, 633
Fu, S. Y., An, J., Zhu, Z. P., et al. 2024, GCN, 36561, 1
Gaia Collaboration, Brown, A. G. A., Vallenari, A., et al. 2018, A&A, 616, A1
Gao, H.-X., Geng, J.-J., Sun, T.-R., et al. 2024, ApJ, 971, 81
Gehrels, N., Chincarini, G., Giommi, P., et al. 2004, ApJ, 611, 1005
Geng, J.-J., Dai, Z.-G., Huang, Y.-F., et al. 2018a, ApJL, 856, L33
Geng, J.-J., Huang, Y.-F., Wu, X.-F., Zhang, B., & Zong, H.-S. 2018b, ApJS, 234, 3
Geng, J. J., Wu, X. F., Huang, Y. F., Li, L., & Dai, Z. G. 2016, ApJ, 825, 107
Geng, J. J., Wu, X. F., Huang, Y. F., & Yu, Y. B. 2013, ApJ, 779, 28
Gezari, S., Jones, D. O., Sanders, N. E., et al. 2015, ApJ, 804, 28
Ghirlanda, G., Nappo, F., Ghisellini, G., et al. 2018, A&A, 609, A112
Giannios, D., & Spitkovsky, A. 2009, MNRAS, 400, 330
Granot, J., & Piran, T. 2012, MNRAS, 421, 570
Gropp, J. D., Dichiara, S., Kennea, J. A., et al. 2024, GCN, 36558, 1
Gu, W.-M., Liu, T., & Lu, J.-F. 2006, ApJL, 643, L87
Hu, L., Wang, L., Chen, X., & Yang, J. 2022, ApJ, 936, 157
Hu, Y. D., Aceituno, F., Fernandez-Garcia, E., et al. 2024, GCN, 36599, 1
Hu, Y.-D., Fernandez-Garcia, E., Caballero-Garcia, M. D., et al. 2023, FrASS, 10, 952887
Huang, Y. F., Dai, Z. G., & Lu, T. 1999, MNRAS, 309, 513
Huang, Y. F., Gou, L. J., Dai, Z. G., & Lu, T. 2000, ApJ, 543, 90
Joshi, J., Waratkar, G., Vibhute, A., et al. 2024, GCN, 36560, 1
Kann, D. A., White, N. E., Ghirlanda, G., et al. 2024, A&A, 686, A56
Kozyrev, A. S., Golovin, D. V., Litvak, M. L., et al. 2024, GCN, 36583, 1
Kumar, A., Gompertz, B. P., Belkin, S., et al. 2024, GCN, 36559, 1
Kumar, P., & Zhang, B. 2015, PhR, 561, 1
Lang, D., Hogg, D. W., Mierle, K., Blanton, M., & Roweis, S. 2010, AJ, 139, 1782
Lasky, P. D., Haskell, B., Ravi, V., Howell, E. J., & Coward, D. M. 2014, PhRvD, 89, 047302
Lee, W. H., Ramirez-Ruiz, E., & López-Cámara, D. 2009, ApJL, 699, L93
Lei, W.-H., Zhang, B., & Liang, E.-W. 2013, ApJ, 765, 125
Lei, W.-H., Zhang, B., Wu, X.-F., & Liang, E.-W. 2017, ApJ, 849, 47
Li, L.-B., Zhang, Z.-B., & Rice, J. 2015, Ap&SS, 359, 37
Liang, E.-W., Yi, S.-X., Zhang, J., et al. 2010, ApJ, 725, 2209
Lim, G., Kim, D., Im, M., et al. 2024, GCN, 36579, 1
Lindegren, L., Hernández, J., Bombrun, A., et al. 2018, A&A, 616, A2
Lipunov, V., Buckley, D., Zhirkov, K., et al. 2024, GCN, 36603, 1
Liu, T., Gu, W.-M., & Zhang, B. 2017, NewAR, 79, 1
Lloyd-Ronning, N. M., Dolence, J. C., & Fryer, C. L. 2016, MNRAS, 461, 1045
Margalit, B., Metzger, B. D., & Beloborodov, A. M. 2015, PhRvL, 115, 171101
Markwardt, C. B., Barthelmy, S. D., Gupta, R., et al. 2024, GCN, 36566, 1
Meyer, E. T., Sparks, W. B., Biretta, J. A., et al. 2013, ApJL, 774, L21
Mo, G., Karambelkar, V., Stein, R., et al. 2024, GCN, 36569, 1
Mohan, T., Swain, V., Salgundi, A., et al. 2024, GCN, 36576, 1
Moskvitin, A. S., Spiridonova, O. I., Vlasyuk, V. V. & GRB follow-up Team 2024, GCN, 36582, 1
Narayan, R., Piran, T., & Kumar, P. 2001, ApJ, 557, 949
Niwano, M., Takahashi, I., Sasada, M., et al. 2024, GCN, 36654, 1

Odeh, M., Guessoum, N., Akl, D., Aabdi, I., & AlShamsi, S. 2024, GCN, 36592, 1
Pankov, N., Pozanenko, A., Klunko, E., Belkin, S. & GRB IKI FuN 2024, GCN, 36585, 1
Pe'er, A. 2012, ApJL, 752, L8
Perez-Garcia, I., Fernandez-Garcia, E., Caballero-Garcia, M. D., et al. 2024, GCN, 36563, 1
Piran, T. 1999, PhR, 314, 575
Piran, T. 2000, PhR, 333, 529
Popham, R., Woosley, S. E., & Fryer, C. 1999, ApJ, 518, 356
Ravi, V., & Lasky, P. D. 2014, MNRAS, 441, 2433
Raynaud, R., Guilet, J., Janka, H.-T., & Gastine, T. 2020, SciA, 6, eaay2732
Rees, M. J., & Mészáros, P. 1994, ApJL, 430, L93
Rhodes, L., Fender, R., Green, D., & Titterington, D. 2024, GCN, 36636, 1
Roming, P. W. A., Kennedy, T. E., Mason, K. O., et al. 2005, SSRv, 120, 95
Ror, A. K., Gupta, A., Rishi, C., Pandey, S. B., & Misra, K. 2024, GCN, 36589, 1
Rossi, A., Maiorano, E., Melandri, A., et al. 2024, GCN, 36655, 1
Sari, R., & Piran, T. 1999, ApJ, 520, 641
Schlafly, E. F., & Finkbeiner, D. P. 2011, ApJ, 737, 103
Shapiro, S. L., & Teukolsky, S. A. 1983, Black Holes, White Dwarfs and Neutron Stars. The Physics of Compact Objects (New York: Interscience)
Shilling, S. P. R., Eyles-Ferris & Swift/UVOT Team 2024, GCN, 36562, 1
Skrutskie, M. F., Cutri, R. M., Stiening, R., et al. 2006, AJ, 131, 1163
Stetson, P. B. 1987, PASP, 99, 191
Stratta, G., Dainotti, M. G., Dall'Osso, S., Hernandez, X., & De Cesare, G. 2018, ApJ, 869, 155
Svinkin, D., Frederiks, D., Ulanov, M., et al. 2024, GCN, 36584, 1
Tan, W., Xiong, S., Li, X., Li, C. & Insight-HXMT Team 2024, GCN, 36578, 1
Tang, C.-H., Huang, Y.-F., Geng, J.-J., & Zhang, Z.-B. 2019, ApJS, 245, 1
Tchekhovskoy, A., Narayan, R., & McKinney, J. C. 2011, MNRAS, 418, L79
Thompson, C. 1994, MNRAS, 270, 480
Tody, D. 1986, Proc. SPIE, 627, 733
Tonry, J. L., Stubbs, C. W., Lykke, K. R., et al. 2012, ApJ, 750, 99
van Eerten, H. 2014, MNRAS, 442, 3495
Vietri, M., & Stella, L. 1998, ApJL, 507, L45
Vinko, J., Sodor, A., Konyves-Toth, R., et al. 2024, GCN, 36577, 1
Wang, T., Liu, G., Cai, Z., et al. 2023, SCPMA, 66, 109512
Wang, X.-G., Zhang, B., Liang, E.-W., et al. 2015, ApJS, 219, 9
Xu, F., Geng, J.-J., Wang, X., Li, L., & Huang, Y.-F. 2022, MNRAS, 509, 4916
Xu, R. X., & Qiao, G. J. 2001, ApJL, 561, L85
Yi, S.-X., Lei, W.-H., Zhang, B., et al. 2017, JHEAp, 13, 1
Yu, Y. W., & Dai, Z. G. 2007, A&A, 470, 119
Yu, Y. W., Liu, X. W., & Dai, Z. G. 2007, ApJ, 671, 637
Zhang, B. 2018, The Physics of Gamma-Ray Bursts (Cambridge: Cambridge Univ. Press)
Zhang, B., Fan, Y. Z., Dyks, J., et al. 2006, ApJ, 642, 354
Zhang, B., & Mészáros, P. 2001, ApJL, 552, L35
Zhang, B., & Yan, H. 2011, ApJ, 726, 90